applied sciences

MDPI

Article

Cu_2ZnSnS_4 Nanoparticles as an Efficient Photocatalyst for the Degradation of Diclofenac in Water

Giorgio Tseberlidis [1,*], Vanira Trifiletti [1,*], Amin Hasan Husien [1], Andrea L'Altrella [1,2], Simona Binetti [1] and Fabio Gosetti [2]

[1] Department of Materials Science, Solar Energy Research Center (MIB-SOLAR), University of Milano-Bicocca, Via Cozzi 55, 20125 Milan, Italy; aminhasan.husien@unimib.it (A.H.H.); a.laltrella@campus.unimib.it (A.L.); simona.binetti@unimib.it (S.B.)

[2] Department of Earth and Environmental Sciences, POLARIS Research Center, University of Milano-Bicocca, Piazza della Scienza 1, 20126 Milan, Italy; fabio.gosetti@unimib.it

* Correspondence: giorgio.tseberlidis@unimib.it (G.T.); vanira.trifiletti@unimib.it (V.T.)

Featured Application: This work has the potential to have a great impact on wastewater treatment plants. The currently adopted methods for the degradation of emerging water micropollutants, such as Diclofenac, are not efficient enough, leading to only 20–40% degradation. Our photocatalyst is a cheap and sustainable tool that allows for up to 90% degradation over 120 min, even when just using visible light sources, meaning it is superior to the dangerous UV-driven photolysis typically observed for this class of compounds.

Abstract: Dangerous emerging water micropollutants like Diclofenac are harming ecosystems all over the planet, and immediate action is needed. The large bandgap photocatalysts conventionally used to degrade them need to be more efficient. Cu_2ZnSnS_4, a well-known light absorber in photovoltaics with a bandgap of 1.5 eV, can efficiently harvest an abundant portion of the solar spectrum. However, its photocatalytic activity has so far only been reported in relation to the degradation of organic dyes, and it is usually used as a benchmark to assess the activity of a photocatalyst without testing its actual potential on a hazardous water micropollutant conventionally encountered in primary and secondary waters. Here, we report the promising photocatalytic activity of Cu_2ZnSnS_4 nanoparticles in the degradation of Diclofenac, chosen as a benchmark for dangerous emerging water micropollutants.

Keywords: photocatalysis; kesterite; Cu_2ZnSnS_4; nanoparticles; wastewaters; water treatment; emerging micropollutants

Citation: Tseberlidis, G.; Trifiletti, V.; Husien, A.H.; L'Altrella, A.; Binetti, S.; Gosetti, F. Cu_2ZnSnS_4 Nanoparticles as an Efficient Photocatalyst for the Degradation of Diclofenac in Water. *Appl. Sci.* **2024**, *14*, 9923. https://doi.org/10.3390/app14219923

Academic Editors: Armando Genco and Riccardo Scarfiello

Received: 26 September 2024
Revised: 17 October 2024
Accepted: 25 October 2024
Published: 30 October 2024

1. Introduction

The degradation of emerging water micropollutants (EWMs) through novel advanced technologies is gaining increasing attention due to the accumulation and persistence of small organic molecules derived from human activity in our ecosystems. The conventional water treatment processes cannot efficiently degrade EWMs, so they frequently undergo natural degradation paths, leading to even more harmful products [1,2]. In recent years, to control water contamination deriving from EWMs, several efforts have been made to find and develop effective, cheap, environmentally friendly, and broad-scope technologies, and among them, we can find advanced oxidation processes, biodegradation, and activated carbon adsorption [3]. However, several issues (like the generation of even more toxic by-products or lack of scalability) have hindered the widespread use of many of these novel technologies. Currently, photocatalysis appears to be the most promising approach for the removal of EWMs. Semiconductor nanoheterostructures for photoconversion applications have been intensively studied in recent years with both experimental and theoretical approaches [4]. They have delivered promising results in many fields,

from photo/electro-catalytic water splitting to CO_2 reduction, as well as from photosynthesis to environmental remediation [5]. The photocatalytic materials conventionally used are represented by common metal oxide semiconductors, and the most representative of them is TiO_2 [6–12]. However, due to their large energy gap, these compounds can only efficiently absorb the UV portion of the solar spectrum, affecting their photocatalytic performance. Kesterite, Cu_2ZnSnS_4 (CZTS), is a p-type semiconductor that is well known in photovoltaics, and it has drawn the scientific community's attention thanks to its excellent absorption coefficient, cost-effectiveness, and environmental sustainability [13,14]. CZTS shows a bandgap of around 1.5 eV, so it can efficiently harvest an abundant portion of the solar spectrum, especially in the visible region [15,16]. Except for PV technologies, this class of semiconductors has been recently reported to be an efficient photocatalyst for organic dye degradation [17–23]. While, for PV applications, CZTS is usually produced by sol–gel methods or high-vacuum depositions [24–33], in the few photocatalytic applications reported, it is mainly provided in the form of nanoparticles or nanocrystals to enhance the contact surface and, therefore, make the active sites easily reachable. Back in 2014, Hou et al. [17] demonstrated how CZTS nanocrystals could efficiently degrade methyl orange, and a few years later, methylene blue was degraded by hydrothermally synthesized CZTS nanoparticles in a study by Phaltane and co-workers [18]. Apostolopoulou et al. also reported excellent photocatalytic efficiencies [19] in a study on the degradation of azo dyes in the presence of nanocrystalline kesterite. More recently, Semalti suggested that the use of CZTS nanocrystals could be considered as a novel approach for the remediation of water from organic pollutants and industrial wastes, but still, only organic dyes have been used to test this system, with there being no development of any analytic methodology to test and assess CZTS photocatalytic activity in the degradation of a truly encountered micropollutant [20]. In another study, Rhodamine B (RhB) was degraded with around 52% efficiency through photocatalysis mediated by a layered microstructure of CZTS synthesized by a hydrothermal method [34]. The same RhB was photodegraded under visible light by Sampath et al. [35] with an efficiency of 79% in 4 h using CZTS films obtained through using chemical spray pyrolysis equipment. Additionally, the CTZS nanoparticles prepared through a solvothermal method by Burhanuz Zaman and co-workers showed an efficiency of 83% in 100 min of RhB degradation under visible light [36]. Furthermore, Wei and co-workers proposed an interesting flower-like CZTS/$Cu_{2-x}S$ structure for their nanoparticles, which degraded 99.8% of the RhB in 100 min, with degradation being carried out using a metal-halide lamp as the light source [37]. So, thanks to the promising results reported regarding dye degradation, as well as its low cost and high stability, CZTS is gaining recognition as an excellent choice in visible-light-driven catalysis. Moreover, its possible application in the photocatalytic degradation of micropollutants, as well as in photo/electro-catalytic hydrogen production reactions [38–40], has promoted CZTS as a material of interest and prompted the research community to focus their efforts in this direction. However, a direct photocatalytic test on a hazardous water micropollutant to test CZTS in a system emulating environmental wastewater has not been reported so far. In this work, we report a direct study on the photocatalytic degradation of Diclofenac (DCF) mediated by CZTS Nanoparticles (NPs). DCF was chosen as a benchmark molecule due to its persistence in ecosystems and its natural photolytic degradation to even more toxic and hazardous carbazoles, assessing it as one of the most dangerous emerging water micropollutants conventionally encountered in primary and secondary waters all over the world. The successful photocatalytic degradation of DCF has been studied and reported, with studies featuring catalysts different from CZTS, such as TiO_2, C_3N_4/ZnO/TiO_2 halloysite nanotubes, g-C_3N_4 nanosheets, MOF/MgAl-hydrotalcite, Nitrogen-Doped Carbon Quantum Dot–Graphitic Carbon Nitride, $BaFe_yTi_{1-y}O_3$, etc. [9,11,12,41–43]. However, these photocatalysts' complex and expensive nature and their need for UV irradiation hinder their potential for widespread use. Here, we not only demonstrate that CZTS NPs are a cheap and active photocatalyst suitable for DCF degradation but also reveal how they are superior to photolysis kinetics when the reaction is performed under UV-vis light irra-

diation, leading to an outstanding result, with 90% of the DCF being degraded. Moreover, the same degradation rates were recorded even with only-visible-light irradiation.

2. Materials and Methods

Diclofenac (DCF) sodic salt powder (pur. $\geq$ 98.5%) was used as purchased from Sigma-Aldrich Corporation (St. Louis, MO, USA). Ultrapure water was produced by using the Milli-Q Elix Essential 15 purification system (Millipore Corporation, Molsheim, France). A 300 W Xenon lamp LSB530 (Quantum Design, San Diego, CA, USA) equipped with a removable UV filter (details in Supplementary Materials; see Figures S1–S3) was used at 1 sun irradiance at the reactor surface (where 1 sun = 1000 W/m^2 at AM1.5) in all the irradiation experiments to better simulate unfiltered and filtered solar radiation. Absorbance spectroscopy measurements were carried out by using a JASCO V-770 UV-visible/NIR spectrophotometer (JASCO International Co., Ltd., Tokyo, Japan) equipped with two different sources (deuterium lamp—190–340 nm; and halogen lamp—340–2500 nm) and SUPRASIL® 10.0 mm 3500 µL volume quartz cuvettes (Hellma GmbH & Co. KG—Müllheim—Germany). XRD measurement was carried out using a Rigaku Miniflex 600 device (FF tube 40 kV, 15 mA, using CuKα radiations at λ= 1.5405 Å) (Rigaku Corporation, Tokyo, Japan). Raman measurements were made through using a Jasco Ventuno µ-Raman instrument at a wavelength of 632.8 nm and a power density of 6 kW/cm^2. TEM measurements were carried out on a JEOL JEM-2100PLUS (JEOL (ITALIA) S.p.A., Basiglio, Italy) with an emission voltage of 200 kV. Samples were prepared by dropping a diluted 0.05 mg/mL solution on a Cu grid. SEM-EDX was performed using Tescan VEGA TS5136XM equipment (Tescan, Brno, Czech Republic).

A DCF standard stock solution (100.0 mg/L) was prepared in ultrapure water and kept at −20°C in an amber glass vial. An aqueous solution of DCF (10.0 mg/L) was freshly prepared for the irradiation experiments. A cylindrical quartz cell (Hellma Italia, Milano, Italy) with a capacity of 28.0 mL was filled with the DCF ultrapure water solution (10.0 mg/L).

For the direct photolysis experiments, the DCF solution was kept under stirring and irradiated by the Xe lamp with or without the UV filter. In contrast, for the catalytic experiments, kesterite nanoparticles (CZTS NPs) (1 g/L) were added to the DCF solution and irradiated by the Xe lamp with or without the UV filter. In each sampling, over the course of the 120 min reaction time, the solution was filtered using a Fisherbrand 0.2 µm hydrophilic PTFE filter before we measured the absorbance.

In this study, standard solutions of DCF (1.0, 2.5, 5.0, and 10.0 mg/L) were prepared to build a calibration plot, reporting the DCF absorbance at 276 nm as the dependent variable y and the standard concentrations as the independent variable x. The quality of the obtained model y = (0.0291 $\pm$ 0.0001)x + (0.0055 $\pm$ 0.0006) was evaluated, obtaining a determination coefficient (R^2) equal to 0.9999.

3. Results and Discussion

This study successfully used a simple and well-known hot-injection method at 280 °C in a N_2 atmosphere to prepare CZTS [44,45]. In a typical experiment, two solutions were prepared for the synthesis process: the first solution (SOL-1) contained all metal precursors and was obtained by dissolving, in a 50 mL three-neck flask, 734 mg $Cu(CH_3COO)_2{\cdot}H_2O$, 439 mg $SnCl_2{\cdot}2H_2O$, and 417 mg $Zn(CH_3COO)_2{\cdot}2H_2O$ in 20 mL of oleylamine (OLA) (in that order); the second solution (SOL-2) contained 128.70 mg of sulfur powder in 10 mL OLA. Both mixtures were connected to a vacuum/N_2 Schlenk line and vacuumed and degassed separately (SOL-2 was degassed for 1 h at 60 °C, while SOL-1 was degassed at 100 °C for 1 h). The SOL-1 flask was then filled with N_2, and the temperature was raised to 190 °C. The mixture was held for 10 min while the mixture color quickly turned from blue to yellow. The temperature was raised to 270 °C, and finally, SOL-2 was rapidly injected into the SOL-1 flask. After the injection process, the reaction mixture immediately changed color from pale yellow to dark brown, and the system was left to react at 270 °C for

30 min. The flask was finally removed from the heating mantle and cooled naturally to room temperature in a N_2 atmosphere. A mixture of chloroform and ethanol (in a ratio of 1:5 v/v) was added to the reaction flask, and the resulting suspension was centrifuged at 8000 rpm for 2 min. The supernatant was eliminated, and this washing step was repeated five times. Finally, the precipitated solid nanoparticles were dried in vacuum and stored under N_2. The so-obtained CZTS NPs were fully characterized through different analytical techniques to ensure their high quality. Based on XRD and Raman measurements, the good quality of the CZTS NPs was proven (Figure 1). Through XRD, only the peaks of CZTS were detectable (DB card number 00–026-0575), with no secondary phases being detectable. In the Raman spectrum, it is possible to see that the CZTS's lone peak slightly shifted to lower wavenumbers, typical of a nanometric crystalline structure [46]. No secondary phases were detected.

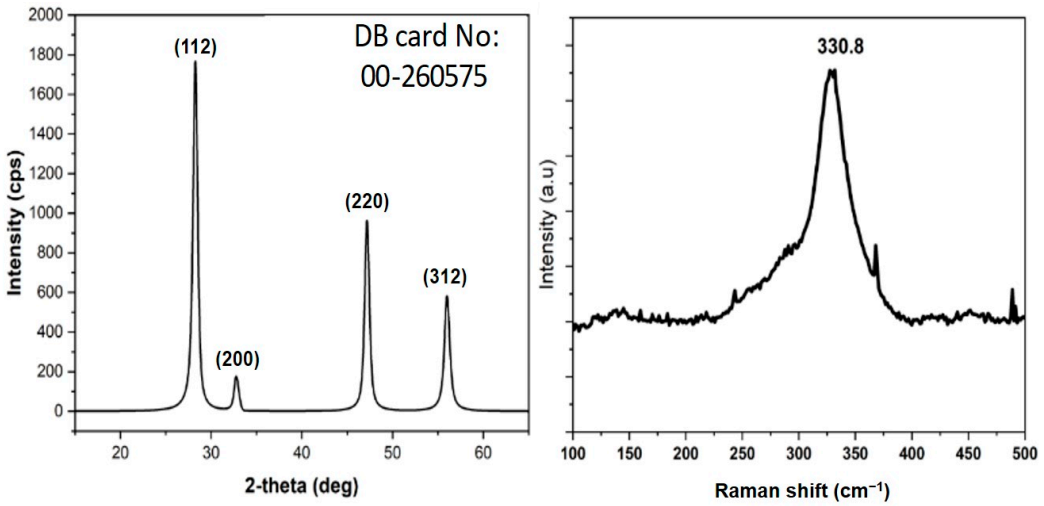

Figure 1. X-ray diffraction (XRD) pattern (**left**) and Raman Spectroscopy (RS) (**right**) of the synthesized Cu_2ZnSnS_4 NPs.

Further characterization was performed using TEM and SEM-EDX measurements. The CZTS NPs had a spherical shape with an average diameter of 11 nm (Figure 2). The resulting elemental ratio perfectly respects the p-type semiconductor Cu_2ZnSnS_4 with copper-poor and zinc-rich condition [47]. Cu/(Zn+Sn) = 0.86, and Zn/Sn = 1.14 (Figure 3).

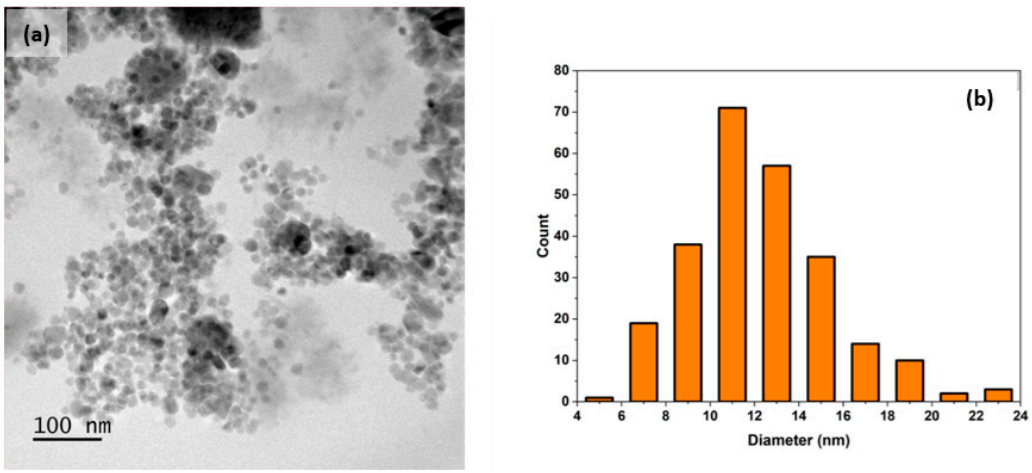

Figure 2. (**a**) TEM image; (**b**) average size distribution of Cu_2ZnSnS_4 NPs. Samples were prepared by dropping a diluted 0.05 mg/mL solution on a Cu grid.

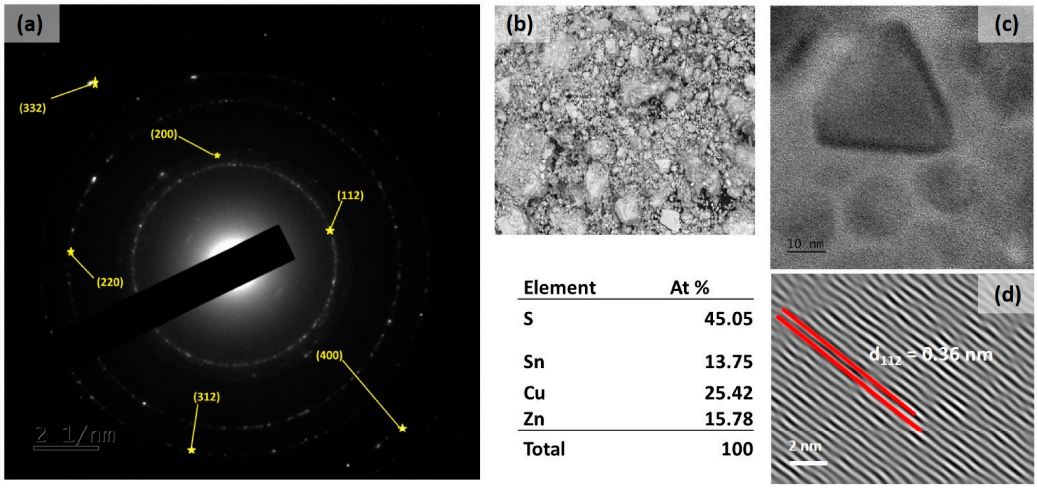

Figure 3. Further Cu_2ZnSnS_4 NPs STEM and elemental content with SEM-EDX characterization. (**a**) Selected area electronic diffraction (SAED) pattern, (**b**) SEM-EDX, (**c**) high-resolution (HR)TEM image, and (**d**) Fast Fourier Transform of the HRTEM image indicating lattice fringes.

The CZTS NPs' photocatalytic activity, by the use of both UV–visible and only visible light, was tested in a water environment and in the presence of low concentrations of DCF, representing one of the most dangerous emerging water micropollutants. The UV-based degradation of DCF through direct photolysis is a well known process, and it has been reported in the literature [48]. This path leads to the formation of a plethora of degradation products. Among them, the derived carbazoles show toxicity and persistence in the environment, which is even more worrying than DCF itself. In this study, first, a possible DCF hydrolysis reaction was evaluated. For this purpose, a 10.0 mg/L DCF solution was kept in the dark and monitored by UV-vis spectroscopy for 120 min, showing no hydrolysis reactions, as depicted in Figure 4.

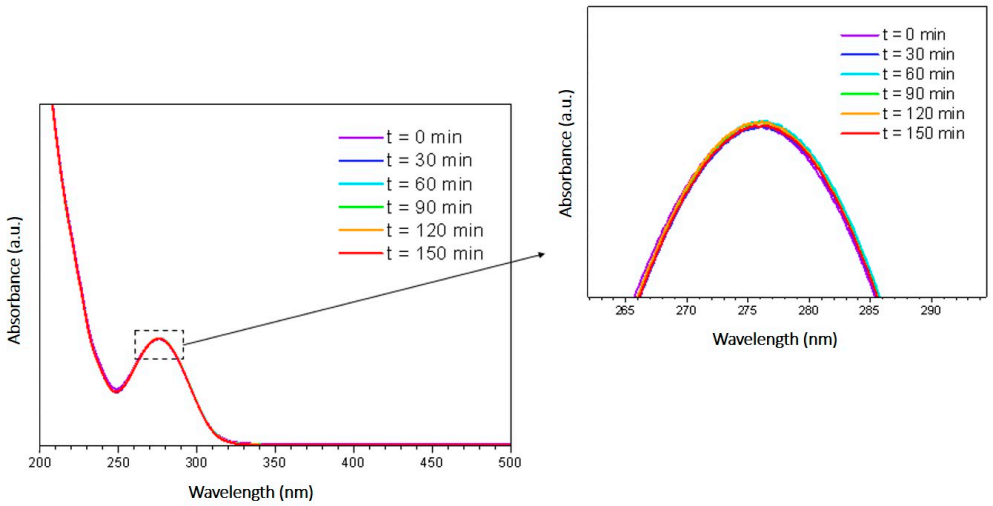

Figure 4. UV-vis absorbance spectra of a 10.0 mg/L DCF solution maintained in the dark at t = 0, 30, 60, 90, 120, and 150 min.

As anticipated, DCF readily undergoes UV photolysis, leading to several toxic by-products, so in the first instance, it was necessary to verify whether this direct photolysis took place in our experimental conditions before checking the activity of the CZTS NP photocatalyst. In Figure 5, it is evident how, after 45 min, the DCF main peak at 276 nm almost disappeared in favor of a new peak located at 235 nm and a broad shoulder peak between 310 and 350 nm, both shifts typical of the carbazole family degradation products [49].

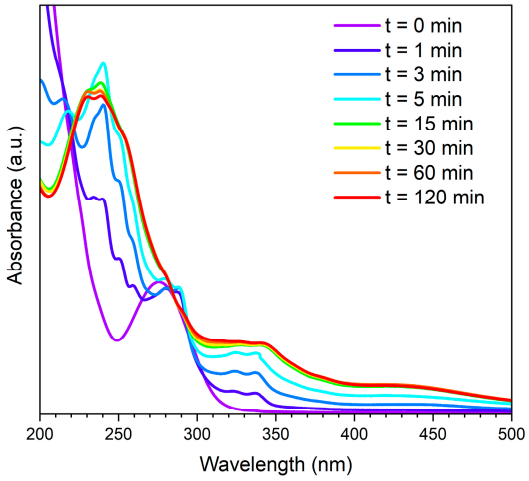

Figure 5. UV-vis absorbance spectra of a 10.0 mg/L DCF solution under 1 sun (1000 W/m^2) irradiance through the use of a 300 W Xenon unfiltered lamp (UV-vis light); t = 0, 1, 3, 5, 15, 30, 60, and 120 min.

Moreover, during photolysis, the solution's appearance also changed gradually, changing from transparent and colorless to slightly turbid and yellow (a color associated with carbazoles), as noted via a simple visual inspection over 120 min (see Figure S5).

The same experiment was repeated by filtering the Xe lamp to verify whether any other degradation path could occur under only visible light irradiation. Figure 6 shows a slight decrease in the DCF peak at 276 nm, indicating that very modest DCF degradation could occur under those conditions. However, no carbazoles were formed, demonstrating that only the UV portion of the light is responsible for that detrimental degradation path.

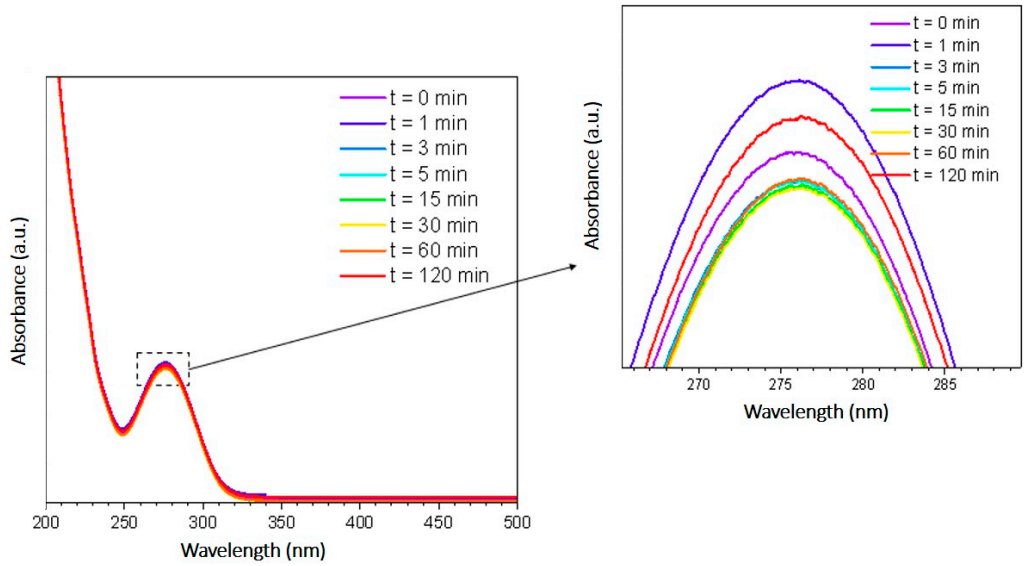

Figure 6. UV-vis absorbance spectra of a 10.0 mg/L DCF solution under 1 sun irradiance through the use of a 300 W Xenon UV-filtered lamp (visible light only); t = 0, 1, 3, 5, 15, 30, 60, and 120 min.

Given the preliminary results regarding DCF photolysis through UV-vis or only visible light, the photocatalytic activity of the CZTS NPs was tested in both the configurations of the Xe lamp, UV-filtered and unfiltered. Regarding the first case, a successful CZTS-mediated photocatalysis method could open up new industrial avenues and facilitate strategies to degrade dangerous water micropollutants such as DCF indoors or directly in dedicated pipelines. For the second case, we wanted to verify whether the photocatalytic path prompted by CZTS NPs could, in any case, prevail over the already fast and natural photolysis of DCF shown previously in Figure 5.

The UV-vis absorbance spectra of two photocatalysis reactions involving a 10.0 mg/L DCF solution, mediated by CZTS NPs (1.0 g/L) under 1 sun irradiance at the reactor surface (where 1 sun = 1000 W/m^2 at AM1.5) through the use of a 300W Xenon unfiltered lamp (UV-vis light, Figure 7a) and UV-filtered lamp (visible light only, Figure 7b) over 120 min, are shown in Figure 7.

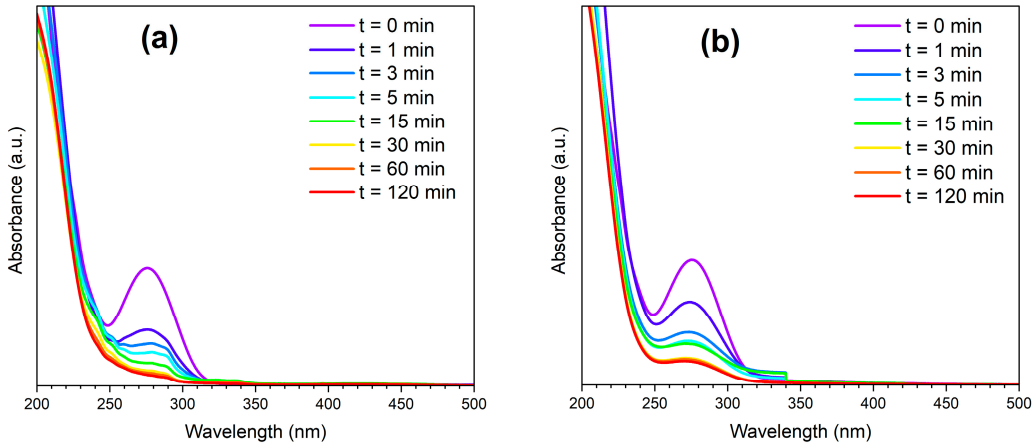

Figure 7. (**a**) UV-vis absorbance spectra of the photocatalysis of a 10.0 mg/L DCF solution mediated by CZTS NPs (1 g/L) under 1 sun irradiance through 300 W Xenon unfiltered lamp (UV-vis light); (**b**) UV-Vis absorbance spectra of the photocatalysis of a 10.0 mg/L DCF solution mediated by CZTS NPs (1 g/L) under 1 sun irradiance through 300 W Xenon UV-filtered lamp (visible light only); t = 0, 1, 3, 5, 15, 30, 60, 120 min.

First, we can observe how the photocatalysis was successful in both cases. Based on Figure 7a, despite the use of the entire light spectrum, including the UV portion, it seems that by the end of the 120 min experiment, DCF was almost completely degraded, with no formation of carbazoles, previously identified in Figure 5 with peaks at 230 nm and a shoulder peak between 310 and 360 nm. It must be pointed out that, during the first few minutes of the photocatalysis (t = 1, 3, 5, and 15 min), traces of by-products were probably formed, as suggested by the shoulders at around 235 nm. However, no other peaks can be detected by the end of the 120 min, indicating that CZTS NPs prevail and degrade the remaining DCF or even the corresponding by-products. Moving to Figure 7b, showing results derived from using visible light only, it is evident how the spectra are more precise, and no other signals seem to be formed during the reaction, suggesting that photocatalysis only involving visible light for DCF degradation could be easily performed indoors or in dedicated industrial setups. Figure 8 shows the trends of the DCF concentration decrease during photocatalytic experiments in the presence of UV-vis light (yellow line and circles) and visible light only (red line and squares) as a function of time. The two trends are very similar, but the decrease in DCF concentration is more significant when irradiated with UV-vis light. Using the same figure, it is also possible to compare photolysis with photocatalysis. In the case of photolysis driven by only visible light (green line, squares), the concentration of DCF remains stable, indicating that no reaction takes place without the aid of a photocatalyst. On the other hand, in UV-vis-light-driven photocatalysis, the apparent slight increase in concentration is just an indirect effect of the newly formed carbazole photolytic products. These carbazoles bring an absorbance peak at 310 nm (as indicated in Figure 5), which is too close to DCF's unique peak at 276 nm to determine DCF's concentration decrease over time. A linear behavior was observed in tests performed with UV-vis and visible light only, indicating linear kinetic models of the second order. The reaction order of the DCF photodegradation was determined by plotting 1/A (with A being the DCF absorbance at 276 nm) against the irradiation time (min). For UV-vis and visible irradiation-only photocatalysis, the determination coefficient (R^2) values were 0.9371 and 0.9776, respectively, and the half-life times ($t_{1/2}$) were 2.1 min and 2.7 min, respectively.

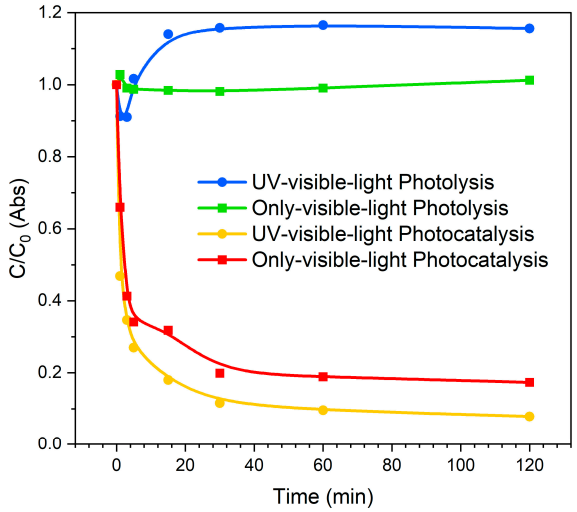

Figure 8. Trends in DCF concentration with respect to the initial value (C/C_0) during the photolysis and photocatalysis experiments with UV-vis light vs. visible light only.

By comparing the two kinetics, it stands out that the residual DCF concentration after 120 min for the visible-light-only photocatalysis (Figure 8, specifically the green lines and circles) is 1.9 (±0.2) mg/L, corresponding to a degradation percentage of the micropollutant of 80 (±10)%. On the other hand, using the entire light spectrum, including the UV portion, the residual DCF concentration after 120 min is 0.8 (±0.1) mg/L, corresponding to a degradation percentage of the micropollutant of 90 (±10)%. However, the two degradation percentages obtained are not significantly different (as shown by a *t*-test at a 95% confidence level). The starting DCF concentration could explain the faster degradation kinetics in the first few minutes. It could be supposed that the reaction proceeds slower when achieving contact between the catalyst and the water-dissolved DCF becomes more difficult due to the DCF being too diluted by the end of the 120 min. Moreover, slight inhibition, due to by-products, of the degradation could occur (i.e., the possible adsorption effect on the NPs that needs to be further investigated), and follow-up work will be conducted to test the catalyst recycle. Further investigations are needed to understand the kinetics mechanism and the nature of the degradation products formed in both cases. However, preliminary results on the investigation of the main degradation product by the end of the 120 min reaction time indicate a molecule at m/z 201 (ESI−) and m/z 203 (ESI+) with the formula $C_8H_{10}O_6$ (Figures 9 and 10). Based on the MS/MS spectrum, the chemical structure of the species is proposed (Figure 11), and it does not belong to the carbazole family.

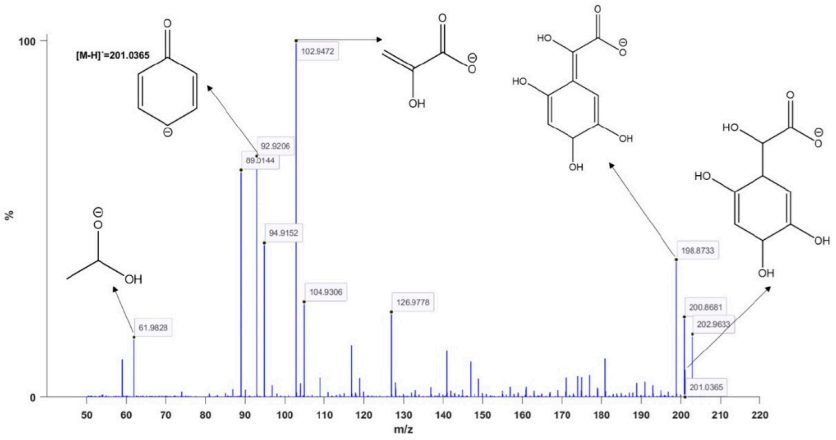

Figure 9. (ESI−) MS/MS spectrum of the main degradation product after 120' reaction time in visible-light-only photocatalysis mediated by Cu_2ZnSnS_4 nanoparticles.

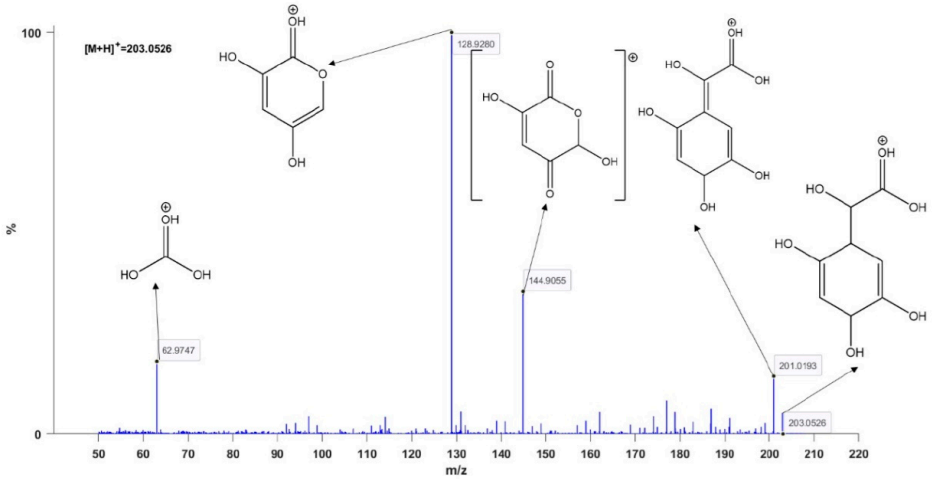

Figure 10. (ESI+) MS/MS spectrum of the main degradation product after 120′ reaction time in visible-light-only photocatalysis mediated by Cu_2ZnSnS_4 nanoparticles.

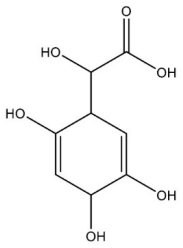

Figure 11. Proposed structure for the main degradation product. MW: 202 g/mol; formula: $C_8H_{10}O_6$.

The outcome of this preliminary photocatalytic study suggests that the DCF degradation reaction proceeds with a typical radical mechanism, as reported for other types of light absorbers [50], and is summarized in Figure 12. The process starts with the CZTS NPs' light absorption, so electron–hole pairs are generated: electrons are promoted from the valence band to the conduction band, leaving holes in the valence band.

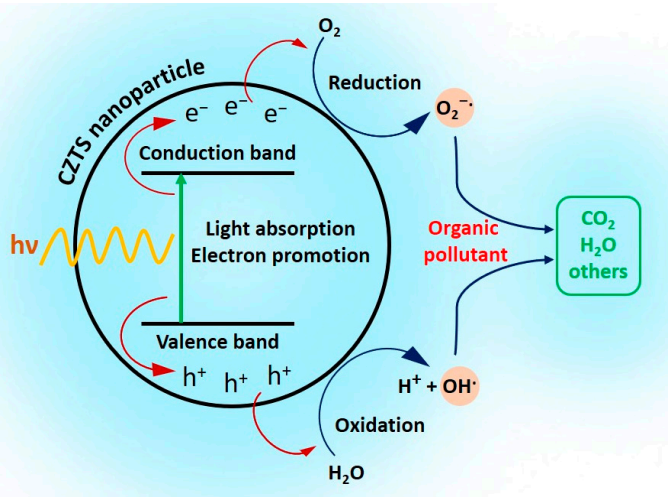

Figure 12. DCF photocatalytic cycle mediated by CZTS NPs.

After the generation of electron–hole pairs, the corresponding charge separation occurs. After the migration of charge carriers, the redox reactions that lead to the degradation of DCF present in the surroundings are promoted. The photogenerated electrons typically reduce electron acceptors, such as oxygen molecules, forming reactive oxygen species (ROS)

like superoxide anions ($O_2^{\bullet -}$). Parallelly, the holes oxidize electron donors, often water or hydroxide ions, to generate hydroxyl radicals ($OH^{\bullet}$). Both radical species are highly reactive and can attack and break down complex organic molecules by bond cleavage, converting them into less harmful or more easily manageable substances. The key advantage of CZTS NPs resides in their narrow bandgap of 1.5 eV. In this way, it is possible to drive the reaction by using only visible light and avoiding other possible degradation paths related to UV photolysis.

These preliminary results are encouraging and could facilitate new ways for wastewater and primary water treatment against emerging micropollutants such as DCF, considering that, nowadays, the DCF degradation in industrial water treatment plants ranges between 20 and 40% [51,52]. Moreover, though CZTS NPs' photocatalytic performance has been reported on and documented in the literature in case studies and reports of proof-of-concept experiments involving organic dyes, to the best of our knowledge, no direct research on a water micropollutant has been reported so far.

4. Conclusions

In conclusion, in this study, we have reported, for the first time, the photocatalytic activity of CZTS NPs in relation to the degradation of wastewater and primary water micropollutants, showing remarkable results. We chose DCF as a benchmark primarily because it is a known and worrying emerging micropollutant due to its natural degradation of harmful and even more toxic carbazoles through photolysis. Secondarily, its main peak in UV-vis spectroscopy at 276 nm allowed for the study of the degradation kinetics. We have demonstrated that CZTS NPs are an active photocatalyst suitable for DCF degradation and that they prevail over photolysis kinetics when the reaction is performed under UV-vis light irradiation, leading to an outstanding 90% of the DCF being degraded, with no carbazole formation taking place. Compared to the photocatalysts featured in other photocatalytic degradation studies reported in the literature, CZTS is a cheap photocatalyst that shows comparable results in terms of degradation rates, but more importantly, CZTS can operate in only-visible-light conditions, obtaining comparable results. Thanks to the visible-light absorption properties of CZTS, our catalytic system demonstrably performs well when irradiating with a visible-light-only source, providing the same performance as under UV-vis light. This also makes our system suitable for indoor applications with visible light sources. We look forward to the possible industrial implementation of this system in dedicated pipelines, especially seeing as it could facilitate improved results compared to the current DCF industrial degradation rates. These preliminary results are promising and could facilitate new ways for wastewater and primary water treatment against emerging micropollutants such as DCF, considering that, nowadays, the DCF degradation rates in industrial water treatment plants range between 20 and 40%. Further investigations are needed to understand the kinetics mechanism and the nature of the degradation products formed. A further step will be identifying the best possible operating conditions to decrease the amount of catalyst used, identifying the lowest/highest DCF concentration degradable with our system, and testing the recycling of CZTS NPs.

Supplementary Materials: The following supporting information can be downloaded at: https://www.mdpi.com/article/10.3390/app14219923/s1. Cu_2ZnSnS_4 nanoparticle preparation; Figure S1: 300 W Xenon lamp LSB530 (Quantum Design, San Die-go, CA, USA); Figure S2: Photolysis and photocatalysis setup; Figure S3: Quantum Design (San Diego, CA, USA) producer's emission spectra; Figure S4: Cu_2ZnSnS_4 nanoparticles used as a photocatalyst; Figure S5: Filtered reaction solution after 120′ of UV-vis and after 120′ of UV-vis photocatalysis.

Author Contributions: Conceptualization, G.T., V.T. and F.G.; methodology, G.T., A.H.H., A.L. and F.G.; validation, G.T., V.T. and F.G.; investigation, G.T., A.H.H. and A.L.; resources, S.B. and F.G.; data curation, G.T. and F.G.; writing—original draft preparation, G.T., V.T. and F.G.; writing—review and editing, G.T., V.T. and F.G.; visualization, G.T. and V.T.; supervision, G.T., V.T., S.B. and F.G.; project administration, S.B. and F.G.; funding acquisition, S.B. All authors have read and agreed to the published version of the manuscript.

Funding: This work was supported by a PhD scholarship on Green Issues from action IV.5 of the PON Research and Innovation 2014–2020 "Education and research for recovery—REACT-EU" program. This work was also supported by the "MUSA—Multilayered Urban Sustainability Action" project, funded by the European Union, via NextGenerationEU, under the National Recovery and Resilience Plan (NRRP) Mission 4 Component 2 Investment Line 1.5: Strengthening of research structures and creation of R&D "innovation ecosystems", set up of "territorial leaders in R&D".

Institutional Review Board Statement: Not applicable.

Informed Consent Statement: Not applicable.

Data Availability Statement: The data supporting this article have been included as part of the Supplementary Materials.

Conflicts of Interest: The authors declare no conflicts of interest.

References

1. Gosetti, F.; Bottaro, M.; Gianotti, V.; Mazzucco, E.; Frascarolo, P.; Zampieri, D.; Oliveri, C.; Viarengo, A.; Gennaro, M.C. Sun Light Degradation of 4-Chloroaniline in Waters and Its Effect on Toxicity. A High Performance Liquid Chromatography—Diode Array—Tandem Mass Spectrometry Study. *Environ. Pollut.* **2010**, *158*, 592–598. [CrossRef] [PubMed]
2. Gosetti, F.; Belay, M.H.; Marengo, E.; Robotti, E. Development and Validation of a UHPLC-MS/MS Method for the Identification of Irinotecan Photodegradation Products in Water Samples. *Environ. Pollut.* **2020**, *256*, 113370. [CrossRef] [PubMed]
3. Qutob, M.; Alshehri, S.; Shakeel, F.; Alam, P.; Rafatullah, M. Insight into Photodegradation of Diclofenac: Mechanism, Efficiency, Role of Parameters, Toxicity Assessment and Catalyst Stability. *Rev. Environ. Contam. Toxicol.* **2023**, *261*, 27. [CrossRef]
4. Lin, C.-H.; Rohilla, J.; Kuo, H.-H.; Chen, C.-Y.; Mark Chang, T.-F.; Sone, M.; Ingole, P.P.; Lo, Y.-C.; Hsu, Y.-J. Density-Functional Theory Studies on Photocatalysis and Photoelectrocatalysis: Challenges and Opportunities. *Sol. RRL* **2024**, *8*, 2300948. [CrossRef]
5. Fang, M.-J.; Tsao, C.-W.; Hsu, Y.-J. Semiconductor Nanoheterostructures for Photoconversion Applications. *J. Phys. D Appl. Phys.* **2020**, *53*, 143001. [CrossRef]
6. Murgolo, S.; Moreira, I.S.; Piccirillo, C.; Castro, P.M.L.; Ventrella, G.; Cocozza, C.; Mascolo, G. Photocatalytic Degradation of Diclofenac by Hydroxyapatite–TiO_2 Composite Material: Identification of Transformation Products and Assessment of Toxicity. *Materials* **2018**, *11*, 1779. [CrossRef]
7. Lara-Pérez, C.; Leyva, E.; Zermeño, B.; Osorio, I.; Montalvo, C.; Moctezuma, E. Photocatalytic Degradation of Diclofenac Sodium Salt: Adsorption and Reaction Kinetic Studies. *Environ. Earth Sci.* **2020**, *79*, 277. [CrossRef]
8. Mugunthan, E.; Saidutta, M.B.; Jagadeeshbabu, P.E. Photocatalytic Degradation of Diclofenac Using TiO_2–SnO_2 Mixed Oxide Catalysts. *Environ. Technol.* **2019**, *40*, 929–941. [CrossRef]
9. Aghababaei, N.; Abdouss, M.; Hosseini-Monfared, H.; Ghanbari, F. Photocatalytic Degradation of Diclofenac Using a Novel Double Z-Scheme Catalyst (O-g-C_3N_4/ZnO/TiO_2@halloysite Nanotubes): Degradation Mechanism, Identification of by-Products and Environmental Implementation. *J. Water Process Eng.* **2023**, *53*, 103702. [CrossRef]
10. Rizzo, L.; Meric, S.; Kassinos, D.; Guida, M.; Russo, F.; Belgiorno, V. Degradation of Diclofenac by TiO_2 Photocatalysis: UV Absorbance Kinetics and Process Evaluation through a Set of Toxicity Bioassays. *Water Res.* **2009**, *43*, 979–988. [CrossRef]
11. Moctezuma, E.; Leyva, E.; Lara-Pérez, C.; Noriega, S.; Martínez-Richa, A. TiO_2 Photocatalytic Degradation of Diclofenac: Intermediates and Total Reaction Mechanism. *Top Catal.* **2020**, *63*, 601–615. [CrossRef]
12. Rodrigues, A.S.; Silveira, J.E.; Carbajo, J.; Zazo, J.A.; Casas, J.A.; Fernandes, A.; Pacheco, M.J.; Ciríaco, L.; Lopes, A. Diclofenac Photodegradation with the Perovskites $BaFe_yTi_{1-y}O_3$ as Catalysts. *Environ. Sci. Pollut. Res.* **2021**, *28*, 23822–23832. [CrossRef] [PubMed]
13. He, M.; Yan, C.; Li, J.; Suryawanshi, M.P.; Kim, J.; Green, M.A.; Hao, X. Kesterite Solar Cells: Insights into Current Strategies and Challenges. *Adv. Sci.* **2021**, *8*, 2004313. [CrossRef] [PubMed]
14. Tseberlidis, G.; Trifiletti, V.; Le Donne, A.; Frioni, L.; Acciarri, M.; Binetti, S. Kesterite Solar-Cells by Drop-Casting of Inorganic Sol–Gel Inks. *Sol. Energy* **2020**, *208*, 532–538. [CrossRef]
15. Maalouf, A.; Okoroafor, T.; Jehl, Z.; Babu, V.; Resalati, S. A Comprehensive Review on Life Cycle Assessment of Commercial and Emerging Thin-Film Solar Cell Systems. *Renew. Sustain. Energy Rev.* **2023**, *186*, 113652. [CrossRef]
16. Sivaraj, S.; Rathanasamy, R.; Kaliyannan, G.V.; Panchal, H.; Jawad Alrubaie, A.; Musa Jaber, M.; Said, Z.; Memon, S. A Comprehensive Review on Current Performance, Challenges and Progress in Thin-Film Solar Cells. *Energies* **2022**, *15*, 8688. [CrossRef]
17. Hou, X.; Li, Y.; Yan, J.-J.; Wang, C.-W. Highly Efficient Photocatalysis of P-Type Cu_2ZnSnS_4 under Visible-Light Illumination. *Mater. Res. Bull.* **2014**, *60*, 628–633. [CrossRef]
18. Phaltane, S.A.; Vanalakar, S.A.; Bhat, T.S.; Patil, P.S.; Sartale, S.D.; Kadam, L.D. Photocatalytic Degradation of Methylene Blue by Hydrothermally Synthesized CZTS Nanoparticles. *J. Mater. Sci. Mater. Electron.* **2017**, *28*, 8186–8191. [CrossRef]
19. Apostolopoulou, A.; Mahajan, S.; Sharma, R.; Stathatos, E. Novel Development of Nanocrystalline Kesterite Cu_2ZnSnS_4 Thin Film with High Photocatalytic Activity under Visible Light Illumination. *J. Phys. Chem. Solids* **2018**, *112*, 37–42. [CrossRef]

20. Semalti, P.; Sharma, V.; Sharma, S.N. A Novel Method of Water Remediation of Organic Pollutants and Industrial Wastes by Solution- Route Processed CZTS Nanocrystals. *J. Mater.* **2021**, *7*, 904–919. [CrossRef]
21. Hou, Z.; Li, Y.; Liu, J.; Shen, H.; Huo, X. The Visible Light-Driven Highly Efficient Photocatalytic Properties of Cu_2ZnSnS_4 Nanoparticles Synthesized by a Hydrothermal Method. *New J. Chem.* **2021**, *45*, 1743–1752. [CrossRef]
22. Alirezazadeh, F.; Alimohammadi, E.; Sheibani, S.; Rashchi, F. A Comparative Study on the Photocatalytic Activity and Formation Mechanism of Nanostructured Cu_2ZnSnS_4 Prepared by Thermal and Mechano-Thermal Methods. *Mater. Chem. Phys.* **2022**, *292*, 126856. [CrossRef]
23. Yang, Y.; Ding, Y.; Zhang, J.; Liang, N.; Long, L.; Liu, J. Insight into the Growth Mechanism of Mixed Phase CZTS and the Photocatalytic Performance. *Nanomaterials* **2022**, *12*, 1439. [CrossRef] [PubMed]
24. Tseberlidis, G.; Hasan Husien, A.; Riva, S.; Frioni, L.; Le Donne, A.; Acciarri, M.; Binetti, S. Semi-Transparent Cu_2ZnSnS_4 Solar Cells by Drop-Casting of Sol-Gel Ink. *Sol. Energy* **2021**, *224*, 134–141. [CrossRef]
25. Trifiletti, V.; Tseberlidis, G.; Colombo, M.; Spinardi, A.; Luong, S.; Danilson, M.; Grossberg, M.; Fenwick, O.; Binetti, S. Growth and Characterization of $Cu_2Zn_{1-x}Fe_xSnS_4$ Thin Films for Photovoltaic Applications. *Materials* **2020**, *13*, 1471. [CrossRef]
26. Tseberlidis, G.; Trifiletti, V.; Vitiello, E.; Husien, A.H.; Frioni, L.; Da Lisca, M.; Alvarez, J.; Acciarri, M.; Binetti, S.O. Band-Gap Tuning Induced by Germanium Introduction in Solution-Processed Kesterite Thin Films. *ACS Omega* **2022**, *7*, 23445–23456. [CrossRef]
27. Wang, W.; Winkler, M.T.; Gunawan, O.; Gokmen, T.; Todorov, T.K.; Zhu, Y.; Mitzi, D.B. Device Characteristics of CZTSSe Thin-Film Solar Cells with 12.6% Efficiency. *Adv. Energy Mater.* **2014**, *4*, 1301465. [CrossRef]
28. Espindola-Rodriguez, M.; Sylla, D.; Sánchez, Y.; Oliva, F.; Grini, S.; Neuschitzer, M.; Vines, L.; Izquierdo-Roca, V.; Saucedo, E.; Placidi, M. Bifacial Kesterite Solar Cells on FTO Substrates. *ACS Sustain. Chem. Eng.* **2017**, *5*, 11516–11524. [CrossRef]
29. Li, X.; Zhuang, D.; Zhang, N.; Zhao, M.; Yu, X.; Liu, P.; Wei, Y.; Ren, G. Achieving 11.95% Efficient $Cu_2ZnSnSe_4$ Solar Cells Fabricated by Sputtering a Cu–Zn–Sn–Se Quaternary Compound Target with a Selenization Process. *J. Mater. Chem. A Mater.* **2019**, *7*, 9948–9957. [CrossRef]
30. Wang, Z.; Wang, Y.; Taghipour, N.; Peng, L.; Konstantatos, G. Ag-Refined Kesterite in Superstrate Solar Cell Configuration with 9.7% Power Conversion Efficiency. *Adv. Funct. Mater.* **2022**, *32*, 2205948. [CrossRef]
31. Wang, Z.; Wang, Y.; Konstantatos, G. Highly Efficient, Ultrathin, Cd-Free Kesterite Solar Cells in Superstrate Configuration Enabled by Band Level Tuning via Ag Incorporation. *Nano Energy* **2022**, *94*, 106898. [CrossRef]
32. Trifiletti, V.; Frioni, L.; Tseberlidis, G.; Vitiello, E.; Danilson, M.; Grossberg, M.; Acciarri, M.; Binetti, S.; Marchionna, S. Manganese-Substituted Kesterite Thin-Films for Earth-Abundant Photovoltaic Applications. *Sol. Energy Mater. Sol. Cells* **2023**, *254*, 112247. [CrossRef]
33. Butrichi, F.; Trifiletti, V.; Tseberlidis, G.; Colombo, B.E.G.; Taglietti, F.; Rancan, M.; Armelao, L.; Binetti, S. Wet Synthesis of Cu_2MnSnS_4 Thin Films for Photovoltaics: Oxidation Control and CdS Impact on Device Performances. *Sol. Energy Mater. Sol. Cells* **2024**, *272*, 112924. [CrossRef]
34. Guo, Y.; Wei, J.; Liu, Y.; Yang, T.; Xu, Z. Surfactant-Tuned Phase Structure and Morphologies of Cu_2ZnSnS_4 Hierarchical Microstructures and Their Visible-Light Photocatalytic Activities. *Nanoscale Res. Lett.* **2017**, *12*, 181. [CrossRef] [PubMed]
35. Sampath, M.; Sankarasubramanian, K.; Archana, J.; Hayakawa, Y.; Ramamurthi, K.; Sethuraman, K. Structural, Optical and Photocatalytic Properties of Spray Deposited Cu_2ZnSnS_4 Thin Films with Various S/(Cu+Zn+Sn) Ratio. *Mater. Sci. Semicond. Process.* **2018**, *87*, 54–64. [CrossRef]
36. Burhanuz Zaman, M.; Mir, R.A.; Poolla, R. Growth and Properties of Solvothermally Derived Highly Crystalline Cu_2ZnSnS_4 Nanoparticles for Photocatalytic and Electrocatalytic Applications. *Int. J. Hydrogen Energy* **2019**, *44*, 23023–23033. [CrossRef]
37. Wei, Q.-B.; Xu, P.; Ren, X.-P.; Fu, F. Flower-like Cu_2ZnSnS_4 Architectures Synthetize and Their Visible-Light Catalytic Properties. *J. Alloys Compd.* **2019**, *770*, 424–432. [CrossRef]
38. Li, L.; Wang, C.; Feng, K.; Huang, D.; Wang, K.; Li, Y.; Jiang, F. Kesterite Cu_2ZnSnS_4 Thin-Film Solar Water-Splitting Photovoltaics for Solar Seawater Desalination. *Cell Rep. Phys. Sci.* **2021**, *2*, 100468. [CrossRef]
39. Ros, C.; Andreu, T.; Giraldo, S.; Izquierdo-Roca, V.; Saucedo, E.; Morante, J.R. Turning Earth Abundant Kesterite-Based Solar Cells Into Efficient Protected Water-Splitting Photocathodes. *ACS Appl. Mater. Interfaces* **2018**, *10*, 13425–13433. [CrossRef]
40. Oueslati, S.; Pilvet, M.; Grossberg, M.; Kauk-Kuusik, M.; Krustok, J.; Meissner, D. Kesterite Monograins for Solar Cells and Water Splitting Applications. *Thin Solid Films* **2021**, *739*, 138981. [CrossRef]
41. Jiménez-Salcedo, M.; Monge, M.; Tena, M.T. The Photocatalytic Degradation of Sodium Diclofenac in Different Water Matrices Using G-C_3N_4 Nanosheets: A Study of the Intermediate by-Products and Mechanism. *J. Environ. Chem. Eng.* **2021**, *9*, 105827. [CrossRef]
42. Wang, J.-H.; Kong, F.; Liu, B.-F.; Zhuo, S.-N.; Ren, N.-Q.; Ren, H.-Y. Enhanced Photocatalytic Degradation of Diclofenac by UiO-66/MgAl-LDH: Excellent Performances and Mechanisms. *Environ. Sci. Nano* **2024**, *11*, 3286–3293. [CrossRef]
43. Awang, H.; Peppel, T.; Strunk, J. Photocatalytic Degradation of Diclofenac by Nitrogen-Doped Carbon Quantum Dot-Graphitic Carbon Nitride (CNQD). *Catalysts* **2023**, *13*, 735. [CrossRef]
44. Khanzada, L.S.; Levchuk, I.; Hou, Y.; Azimi, H.; Osvet, A.; Ahmad, R.; Brandl, M.; Herre, P.; Distaso, M.; Hock, R.; et al. Effective Ligand Engineering of the Cu_2ZnSnS_4 Nanocrystal Surface for Increasing Hole Transport Efficiency in Perovskite Solar Cells. *Adv. Funct. Mater.* **2016**, *26*, 8300–8306. [CrossRef]

45. Steinhagen, C.; Panthani, M.G.; Akhavan, V.; Goodfellow, B.; Koo, B.; Korgel, B.A. Synthesis of Cu_2ZnSnS_4 Nanocrystals for Use in Low-Cost Photovoltaics. *J. Am. Chem. Soc.* **2009**, *131*, 12554–12555. [CrossRef]
46. Podsiadlo, S.; Bialoglowski, M.; Fadaghi, M.; Gebicki, W.; Jastrzebski, C.; Zero, E.; Trzybinski, D.; Wozniak, K. Synthesis of Magnetic Doped Kesterite Single Crystals. *Cryst. Res. Technol.* **2015**, *50*, 690–694. [CrossRef]
47. Ito, K. *Copper Zinc Tin Sulfide-Based Thin Film Solar Cells*; John Wiley & Sons: Hoboken, NJ, USA, 2015.
48. Musa, K.A.K.; Eriksson, L.A. Photodegradation Mechanism of the Common Non-Steroid Anti-Inflammatory Drug Diclofenac and Its Carbazole Photoproduct. *Phys. Chem. Chem. Phys.* **2009**, *11*, 4601–4610. [CrossRef]
49. Aparici-Espert, I.; Miranda, M.A.; Lhiaubet-Vallet, V. Sunscreen-Based Photocages for Topical Drugs: A Photophysical and Photochemical Study of A Diclofenac-Avobenzone Dyad. *Molecules* **2018**, *23*, 673. [CrossRef]
50. Chiu, Y.-H.; Chang, T.-F.M.; Chen, C.-Y.; Sone, M.; Hsu, Y.-J. Mechanistic Insights into Photodegradation of Organic Dyes Using Heterostructure Photocatalysts. *Catalysts* **2019**, *9*, 430. [CrossRef]
51. Verlicchi, P.; Al Aukidy, M.; Zambello, E. Occurrence of Pharmaceutical Compounds in Urban Wastewater: Removal, Mass Load and Environmental Risk after a Secondary Treatment—A Review. *Sci. Total Environ.* **2012**, *429*, 123–155. [CrossRef]
52. Lonappan, L.; Brar, S.K.; Das, R.K.; Verma, M.; Surampalli, R.Y. Diclofenac and Its Transformation Products: Environmental Occurrence and Toxicity—A Review. *Environ. Int.* **2016**, *96*, 127–138. [CrossRef] [PubMed]